

# RSC Advances



This is an *Accepted Manuscript*, which has been through the Royal Society of Chemistry peer review process and has been accepted for publication.

*Accepted Manuscripts* are published online shortly after acceptance, before technical editing, formatting and proof reading. Using this free service, authors can make their results available to the community, in citable form, before we publish the edited article. This *Accepted Manuscript* will be replaced by the edited, formatted and paginated article as soon as this is available.

You can find more information about *Accepted Manuscripts* in the [Information for Authors](#).

Please note that technical editing may introduce minor changes to the text and/or graphics, which may alter content. The journal's standard [Terms & Conditions](#) and the [Ethical guidelines](#) still apply. In no event shall the Royal Society of Chemistry be held responsible for any errors or omissions in this *Accepted Manuscript* or any consequences arising from the use of any information it contains.

# Gas adsorption on MoS<sub>2</sub>/WS<sub>2</sub> in-plane heterojunction and the I-V response: A first principles study

Jie Sun,<sup>a</sup> Na Lin,<sup>a,\*</sup> Hao Ren,<sup>b,\*</sup> Cheng Tang,<sup>a</sup> Letao Yang,<sup>a</sup> Xian Zhao<sup>a,\*</sup>

<sup>a</sup> State Key Laboratory of Crystal Materials, Shandong University, 250100 Jinan, Shandong, PR China

<sup>b</sup> State Key Laboratory of Heavy Oil Processing & Center for Bioengineering and Biotechnology, China University of Petroleum (East China), 266580 Qingdao, PR China

\*Corresponding authors: [linnakth@gmail.com](mailto:linnakth@gmail.com),  
[renh@upc.edu.cn](mailto:renh@upc.edu.cn),  
[xianzhao@sdu.edu.cn](mailto:xianzhao@sdu.edu.cn).

## ABSTRACT

New artificial in-plane heterojunctions based on two-dimensional transition metal dichalcogenides fabricated in recent reports are considered to be able to offer great scope for applications. Here, we study by first principles calculations the adsorption of CO, H<sub>2</sub>O, NH<sub>3</sub>, NO, and NO<sub>2</sub> gas molecules on the MoS<sub>2</sub>/WS<sub>2</sub> heterojunction. We have determined the optimal adsorption positions and the adsorption strength, which is driven by charge transfer between the molecules and the heterojunction. Except NH<sub>3</sub>, which performs as the charge donor, all the other studied molecules act as charge accepters to the heterojunction. The charge transfer mechanism has been discussed by analyzing the electronic structure of the molecules and the heterojunction. Further calculations show that the molecule adsorption significantly affects the electronic transport properties of the heterojunction. Both the rectification behavior and the value of the passing current can be altered by adsorption, and such sensitivity to adsorption makes the heterojunction a superior gas sensor that promises wide-ranging applications.

**Keywords:** First principles; MoS<sub>2</sub>/WS<sub>2</sub> heterojunction; Gas adsorption; Electronic structure; Electron transport

## 1. INTRODUCTION

Graphene, a two dimension (2D) material, has drawn a significant attention due to its peculiar physical properties and potential applications<sup>1-3</sup>. However, the zero band gap nature of graphene limits its applications in logic electronics. Therefore, a great deal of effort has been made to search for 2D alternatives as replacements<sup>4-6</sup>. Transition metal dichalcogenides (TMDs), such as MoS<sub>2</sub>, WS<sub>2</sub>, have attracted great interests because of its intrinsic band gap and their superior optoelectronic properties<sup>7-9</sup>. The presence of a band gap makes them to be promising candidates for future electronic devices and allows them fabricated as transistors that can be tuned and used as switches, logic circuits and amplifiers<sup>10-12</sup>. For instance, it was reported recently that a field-effect transistor (FET) constructed by monolayer/ few-layer MoS<sub>2</sub> possesses a room-temperature current with an on/off ratio exceeding 10<sup>8</sup> and mobility of 200 cm<sup>2</sup>V<sup>-1</sup>s<sup>-1</sup>.<sup>13</sup>

In parallel with the study of the isolation of TMDs materials, in-plane heterojunctions consisting of two TMD monolayers stitched together have also gained much attention. Previous theoretical studies has revealed that some TMD monolayers and their heterojunctions can align their band structures to be suitable for potential applications in spontaneous water splitting, photovoltaics, and optoelectronics<sup>14-15</sup>. Recently, in-plane heterojunctions including MoS<sub>2</sub>/WS<sub>2</sub>, MoSe<sub>2</sub>/WSe<sub>2</sub> and WS<sub>2</sub>/WSe<sub>2</sub> have been fabricated by means of chemical vapor deposition (CVD)<sup>16-19</sup>. These heterojunctions greatly enhances localized photoluminescence and can be served as intrinsic monolayer p-n junctions with rectification ratios as high as two orders of magnitude. Further electrical transport measurements demonstrated that the heterojunctions could be used to create complementary inverters with high voltage gain.

2D TMDs are suitable for FET sensor applications to detect environmental pollution due to their large surface-to-volume ratio<sup>20-23</sup>. Both theoretical and experimental investigations have demonstrated that the monolayer MoS<sub>2</sub> and WS<sub>2</sub> sheets are sensitive detectors for NH<sub>3</sub>, NO, NO<sub>2</sub> gas molecules<sup>24-30</sup>. This utilization is

mainly based on the change in the resistivity due to molecules adsorption, where charge transfer occurs at the molecule-substrate interface. It is expected that the electrical resistivity and rectification effect of the lateral TMD heterojunctions would be affected by molecules adsorbed especially on their in-plane interface. Hence, it is desirable to explore and establish the trends and rules of gas molecule adsorption on heterojunctions which can be used as high-efficiency sensors, and distinct characteristics of the influence of the molecules on transport behavior.

In this paper, we carried out first principles calculations for the CO, H<sub>2</sub>O, NH<sub>3</sub>, NO and NO<sub>2</sub> molecules, adsorbed on the in-plane MoS<sub>2</sub>/WS<sub>2</sub> heterojunction. Their preferential binding configurations were identified and the charge transfer mechanism is revealed. We also examined the response of electron transport properties of the heterojunction upon the molecular adsorption. This response might be utilized as potential gas sensors.

## 2. COMPUTATIONAL DETAILS

All the electronic structure calculations were carried out based on density functional theory (DFT) with the projector-augmented wave (PAW) method, as implemented in the Vienna ab initio simulation package (VASP)<sup>31</sup>. The generalized gradient approximation (GGA)<sup>32</sup> functional of Perdew, Burke and Ernzerhof (PBE) is used to approximate the exchange and correlation interactions. The van der Waals (vdW) correction proposed by Grimme (DFT-D2)<sup>33</sup> is chosen to describe the long-range interaction. The local density approximation (LDA) is also adopted in some calculations for comparison. A cutoff energy of 400 eV for the plane-wave basis set and a Monkhorst-Pack mesh of 4×6×1 for the Brillouin zone integration were employed. A vacuum layer larger than 15 Å is used to avoid interaction between neighboring images. All the structures were fully relaxed by using the conjugate gradient method until the maximum Hellmann-Feynman forces acting on each atom is less than 0.02 eV/Å. Spin polarization was included in the calculations of the adsorption of NO and NO<sub>2</sub> since these molecules are paramagnetic but not considered in other calculations. By means of Bader analysis, charge transfer between the

monolayer substrate and the adsorbate is obtained.

Electron transport properties are computed of the optimized structures using the nonequilibrium Green's function (NEGF) method implemented in the TRANSIESTA program<sup>34</sup>. The current through the system is calculated according to the Landauer–Büttiker formula:

$$I = G_0 \int T(E, V) [f_L(E) - f_R(E)] dE$$

where  $G_0 = 2e^2/h$  is the unit of quantum conductance,  $T(E, V)$  is the transmission coefficient at energy  $E$  and the bias voltage  $V$ ,  $f_L(E)$  and  $f_R(E)$  are the Fermi distribution functions respectively at left and right electrodes. The k-point samplings for the transmission spectra calculations are respectively 1, 100, and 100 in the x, y, z directions.

To evaluate the stability of the adsorption of gas molecules on the heterojunction, the adsorption energy is defined as

$$E_a = E_{gas/heterojunction} - E_{gas} - E_{heterojunction}$$

where  $E_{gas}$ ,  $E_{heterojunction}$  and  $E_{gas/heterojunction}$  are the total energy of the gas molecule, heterojunction and the adsorbate-substrate system, respectively. A negative value indicates the adsorption of gas molecules on the surface of heterojunction is energetically favorable.

### 3. RESULTS AND DISCUSSION

To model the in-plane MoS<sub>2</sub>/WS<sub>2</sub> heterojunction, a supercell with lattice dimensions of 33.061 Å × 9.542 Å is used (Figure 1), this supercell consists of two individual MoS<sub>2</sub> and WS<sub>2</sub> grains stitched along the zigzag direction, which has been observed previously by Gong<sup>16</sup> et al. The gas molecules were placed on different sites near the interface of the heterojunction, followed by fully relaxation of the adsorption configuration. We present two most stable configurations of each molecule adsorption except NH<sub>3</sub> in Figure 1. The corresponding adsorption energies ( $E_a$ ), equilibrium height ( $d$ ), and charge transfer ( $\Delta Q$ ) upon adsorption calculated with LDA, GGA and PBE+D2 are listed in Table 1. The equilibrium height is defined as the vertical

distance between the lowest atom of the gas molecule and the top S-layer of the heterojunction.

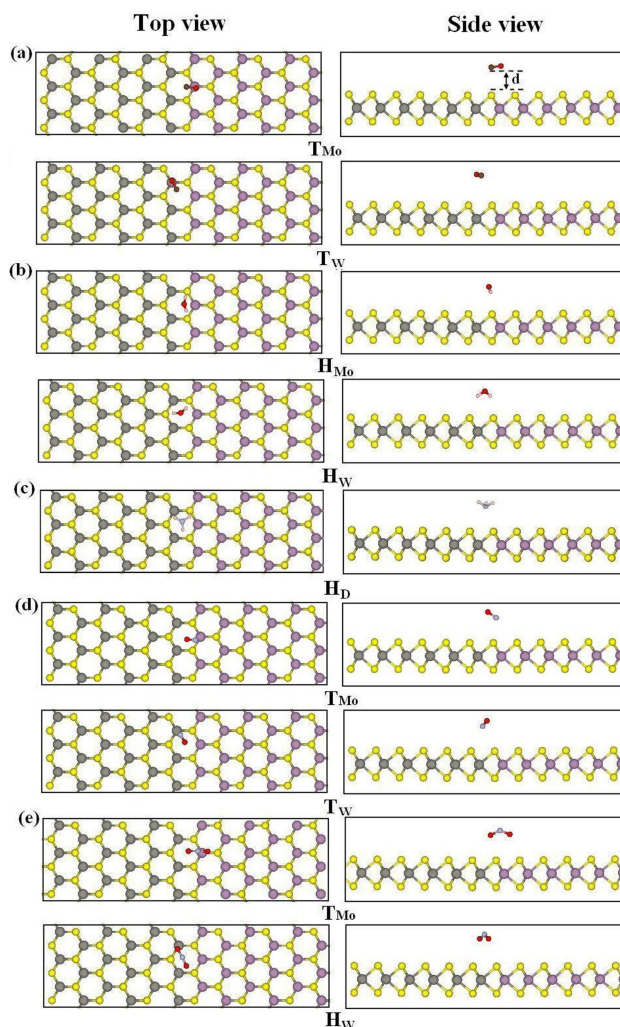


Figure 1. Top (left panel) and side view (right panel) of the favorable configurations for (a)CO, (b)H<sub>2</sub>O, (c)NH<sub>3</sub>, (d) NO, and (e)NO<sub>2</sub> on the heterojunction, respectively.

As previously mentioned, GGA functional cannot account for long-range electron correlation effects and they tend to underestimate weak interactions such as vdW interactions. A pragmatic method to work around this problem has been given by the DFT-D2 approach<sup>33</sup>, which has been previously applied for weak interacting systems finding a good agreement of the theoretical results with the experimental ones<sup>22, 35</sup>. Indeed, all these adsorption energies are significantly increased when the vdW interactions are included, but small changes are found in distances and charge transfer values, as can be seen from Table 1. Different from GGA functional that

underestimates the adsorption energy, LDA functional usually has a tendency to overestimate it. As listed in Table 1, the adsorption energies obtained by using LDA functional are even larger than using PBE+D2 method, due to error cancellation between exchange and correlation effects<sup>36</sup>. Meanwhile, LDA calculations predicted shorter distances and higher charge transfer values compared with GGA and PBE+D2 results. Since both LDA and GGA cannot capture the van der Waals (vdW) interactions in weakly bonded systems, the following discussions about the adsorption properties are based on the PBE+D2 calculated results.

*Table 1. Calculated adsorption energies of the molecules studied with LDA, PBE and PBE with vdW correction.*

Model	Site	LDA			GGA-PBE			PBE+D2		
		Ea (eV)	d (Å)	ΔQ (e)	Ea (eV)	d (Å)	ΔQ (e)	Ea (eV)	d (Å)	ΔQ (e)
CO	T <sub>Mo</sub>	-0.1201	2.8257	-0.0134	0.0087	3.2351	-0.0094	-0.0901	3.2353	-0.0095
	T <sub>W</sub>	-0.1185	2.8774	-0.0111	-0.0017	3.4805	-0.0071	-0.0875	3.4809	-0.0072
H <sub>2</sub> O	H <sub>Mo</sub>	-0.2281	2.2161	-0.0235	-0.0355	2.5635	-0.0165	-0.1527	2.5346	-0.0165
	H <sub>W</sub>	-0.2401	2.2052	-0.0116	-0.0351	2.7989	-0.0119	-0.1555	2.5878	-0.0154
NH <sub>3</sub>	H <sub>D</sub>	-0.1864	2.7075	0.0427	-0.0286	2.9638	0.0234	-0.1585	2.9587	0.0233
NO	T <sub>Mo</sub>	-0.2169	2.2240	-0.0031	-0.0219	2.9083	-0.0050	-0.1224	2.9060	-0.0253
	T <sub>W</sub>	-0.1870	2.4269	-0.0112	-0.0103	2.8988	-0.0038	-0.1196	2.9002	-0.0040
NO <sub>2</sub>	T <sub>Mo</sub>	-0.5509	2.4097	-0.1132	-0.0103	2.9361	-0.0540	-0.1614	2.8932	-0.0546
	T <sub>W</sub>	-0.5431	2.5222	-0.1093	-0.0283	3.3439	-0.0336	-0.1525	3.2135	-0.0405

The calculated results indicate that the CO and NO prefer to locate at the on-top site of the transition metal atoms. H<sub>2</sub>O is stably adsorbed on the hollow site with two hydrogen atoms pointing toward the surface whereas the oxygen atom resides close to one of the transition metal atoms. The NH<sub>3</sub> molecule also prefers to adsorb at the hollow site with the nitrogen atom pointing to the surface. For NO<sub>2</sub> molecule adsorption, the two stable configurations are different, one with NO<sub>2</sub> located at the on-top site of the Mo atom and in the other configuration it is adsorbed at the hollow site with one oxygen atom close to the W atom. In addition, we observed that the adsorption of CO, NO and NO<sub>2</sub> molecules are more stable as close to Mo atom than those close to W atom, although the discrepancies of the adsorption energies are small

(less than 6%). However, for H<sub>2</sub>O molecule, the adsorption configuration near W atom (-0.1555eV) is more stable compared with that near Mo atom (-0.1527eV). There is only one stable configuration for NH<sub>3</sub> adsorption, in which the NH<sub>3</sub> molecule locates at the center of the puckered honeycomb, with adsorption energy of -0.1585 eV. It is worth to note that CO adsorption is the weakest while other molecules exhibit much stronger adsorption energies, especially NO<sub>2</sub>, which has the largest adsorption energy (-0.1614 eV) among the gas molecules studied in the present work. This indicates that the heterojunction is more sensitive to NO<sub>2</sub>, which is similar to the previous results for gas molecular adsorption on graphene and MoS<sub>2</sub><sup>21, 30</sup>.

Bader charge analysis is performed to examine the charge transfer upon adsorption. It is found that most molecules studied are charge acceptors with 0.007 ~ 0.055e transferred from the heterojunction, except NH<sub>3</sub> behaves as a charge donor, providing 0.0233e to the heterojunction. The amount of transferred charge can be correlated with the adsorption energy and the adsorption distance. Strong charge transfer usually corresponds to higher adsorption energy and shorter adsorption distance for the same molecule adsorbed at different positions of the heterojunction. These results are similar to the previous reports on the adsorption of gas molecules on graphene<sup>21</sup> and carbon nanotube<sup>37</sup>, where the gas molecules also behave as either charge acceptors or donors. Recently, in situ photoluminescence measurements also confirmed the donor and acceptor nature of NH<sub>3</sub> and NO<sub>2</sub> adsorption<sup>28</sup>. The charge transfer between the molecule and the heterojunction is expected to have a great impact on the electronic and transport properties of the heterojunction.

Besides the gas molecules adsorbed on the interface of the heterojunction, the adsorption energies of the molecules away from the interface are also calculated with different functionals as shown in Figure 2. It can be seen from Figure 2 that both LDA and GGA-PBE calculations indicate the molecules adsorbed on the interface are more stable than those on the region away from it. As the vdW interaction involved, the most favorable adsorption sites shift to WS<sub>2</sub> region. We should notice that the molecules adsorbed on WS<sub>2</sub> have different adsorption strength comparing with those on MoS<sub>2</sub>. This asymmetric adsorption energy may cause the nonuniform distribution

of the molecule on the heterojunction, which probably also have great influence on the electronic and transport properties of the heterojunction. However, further discussions upon this point are out of the scope of present paper, where we will concentrate on the case of the molecule adsorbed on the interface.

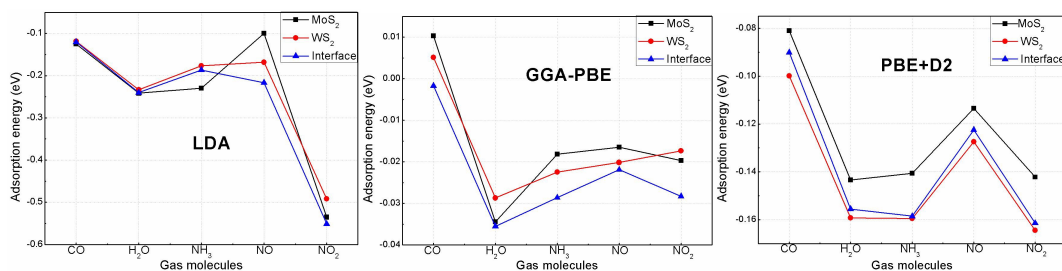
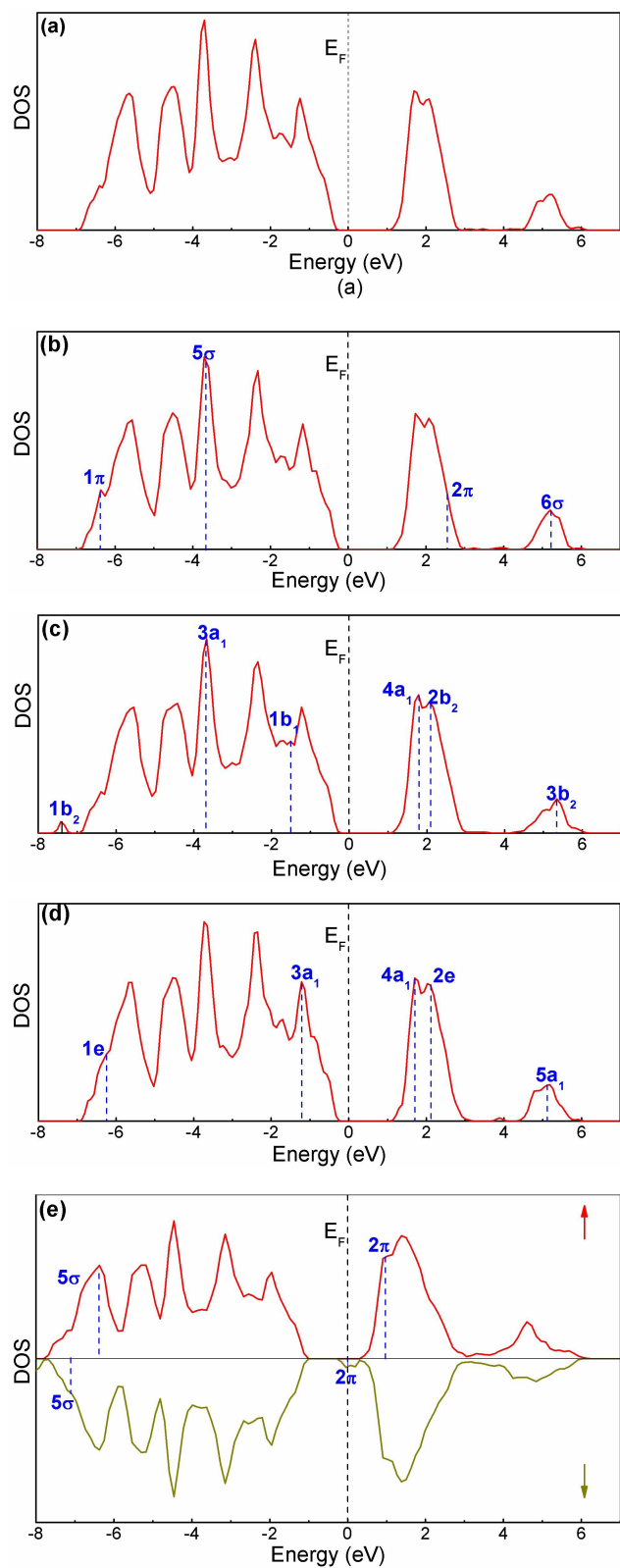


Figure 2. The adsorption energies of the molecules adsorbed on different positions of the heterojunction with different functionals.

In the following part, we shift our focus on the effects of gas adsorption on the electronic properties of the heterojunction. We carried out non-spin polarized calculations for nonmagnetic molecules CO, H<sub>2</sub>O, and NH<sub>3</sub> and spin polarized calculations for paramagnetic molecules NO and NO<sub>2</sub>. The corresponding density of states (DOS) of the most stable configurations and the positions of important molecule orbitals are displayed in Figure 3. The adsorption of nonmagnetic molecules CO, H<sub>2</sub>O, and NH<sub>3</sub> does not substantially affect the valence or conduction band of the heterojunction near the Fermi level (Figure 3 (a)-(d)). This can be attributed to the fact that the positions of these molecules' orbitals are far away from the Fermi level, which only hybrid with deeper states. The mixing orbitals cause the charge transfer between the molecules and the heterojunction, but produce no noticeable modifications of the DOS near the Fermi level.



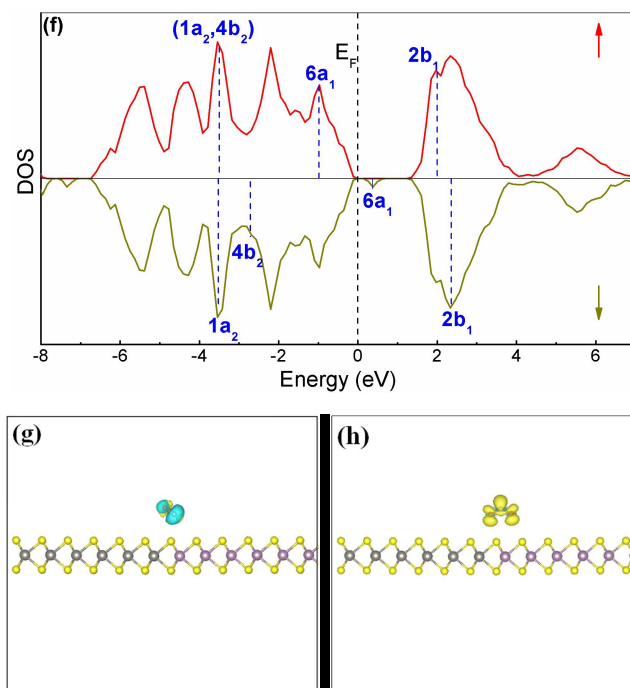
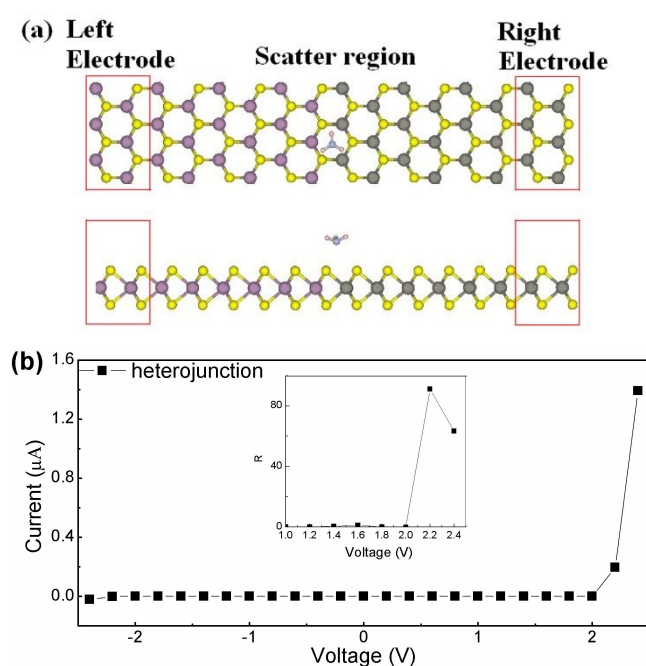


Figure 3. Total DOS of heterojunction (a) with each gas molecule adsorption (b) CO, (c) H<sub>2</sub>O, (d) NH<sub>3</sub>, (e) NO and (f) NO<sub>2</sub>. The blue dotted lines show the positions of the molecular orbitals. The Fermi level is shifted to zero indicated by the black dashed lines. (g), (h) show the spatial spin density distribution on NO and NO<sub>2</sub> molecules.

The adsorption of paramagnetic molecules NO and NO<sub>2</sub> introduces new states near the Fermi level. For NO adsorption (Figure 3(e)), the total magnetic moment is  $-1.0 \mu_B$ . A spin-down impurity state derived from the lowest unoccupied molecular orbital (LUMO) of NO appears at the Fermi level. Since charge transfer occurs when the energies of the valence (conductance) band of the substrate match the LUMO (HOMO) of the molecules. In the case of the molecular HOMO is higher than the substrate Fermi level, charge transfers from the molecule to the substrate, and charge transfers in the opposite direction when the molecular LUMO is lower than the substrate Fermi level. Charge transfer is also affected by the mixing of the molecular HOMO/LUMO with the substrate states. We note that the LUMO ( $2\pi, \downarrow$ ) of NO is located 0.2 eV below the substrate Fermi level. As the consequence, charge transfers from the heterojunction to the molecule. Adsorption of NO<sub>2</sub> on the heterojunction (Figure 3(f)) leads to a magnetic moment of  $1 \mu_B$ , and the Fermi level shifts downwards to the top of the valence band, indicating a hole doping to the heterojunction. The charge transfer from the heterojunction to the molecule can be

caused by the orbital mixing especially the highest occupied molecular orbital (HOMO) ( $6a_1, \uparrow$ ). However, we also notice that the LUMO ( $6a_1, \downarrow$ ) is located at 0.4 eV above the Fermi level, which cause some charge transfer in the opposite direction. The latter charge transfer is relatively weaker and these two effects in total lead to a net charge transfer from the heterojunction to the molecule. The real space distribution of the spin density depicted in Figure 3(g) and 3(h), respectively, illustrate that the spin-polarized electrons are mainly located at the NO or NO<sub>2</sub> molecules in both cases.

Although the adsorption of CO, H<sub>2</sub>O, and NH<sub>3</sub> does not substantially affect the electronic structures of the heterojunction, the charge transfer upon adsorption is expected to vary the electron transport characteristics due to hole or electron doping. These effects are potentially applicable as gas sensors. In order to explicitly evaluate the performance of the heterojunction as a gas sensor, a two-probe system, as shown in Figure 4 (a), where two semi-infinite electrodes are connected with the central scattering region, is employed to calculate the electron transport properties at nonquilibrium conditions. The corresponding current-voltage (I–V) characteristics and their response upon gas molecule adsorption are examined. We selected two representative cases of gas adsorption on heterojunction (NH<sub>3</sub>, non-spin-polarized; and NO<sub>2</sub>, spin-polarized in our electron transport simulation.



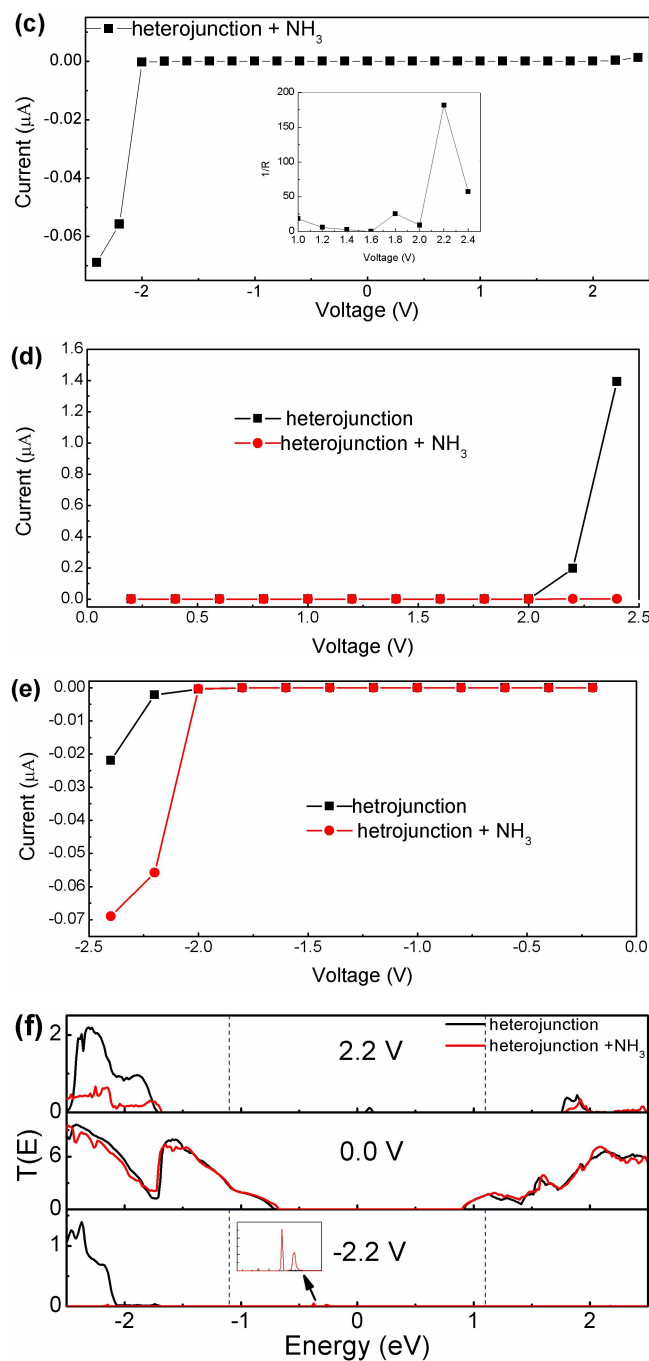


Figure 4. (a) Two-probe systems where semi-infinite left and right electrode regions are in contact with the central scattering region, the upper panel is top view, while the lower one is side views. (b) and (c) The  $I$ - $V$  curve of the heterojunction without and with  $\text{NH}_3$  adsorption, respectively. The rectification ratio  $R(V)$  is shown in the insets. (d) and (e) The  $I$ - $V$  curve of the heterojunction without and with  $\text{NH}_3$  adsorption in positive and negative bias region, respectively. (f) Transmission spectra in  $0$  V and  $\pm 2.2$  V. The blue dashed lines indicate the bias window for the transportation.

The I-V characteristic of the bare heterojunction is shown in figure 4(b). The junction remains switched off for bias voltage below 2.0 V, and switched on above. As the bias voltage further increases, we noticed that the current through the heterojunction in positive bias region is larger than that in the negative bias region, implying a good rectification character. This asymmetric feature of the I-V curve is quantified by a rectification ratio defined as  $R(V) = |I(V)/I(-V)|$ . We found that the R for the heterojunction at 2.2 V is 90 which is close to the experiment result<sup>16</sup> where the current at positive bias is two orders of magnitude higher than the reversed. It is interesting that, when NH<sub>3</sub> is adsorbed on the junction, the rectifying direction is inversed, as shown in figure 4(c). Moreover, the rectifying effect is greatly improved upon NH<sub>3</sub> adsorption, with a rectification ratio of ~190. However, the current of the heterojunction with NH<sub>3</sub> is significantly decreased compared with that without NH<sub>3</sub> in the positive bias region (figure 4(d)). The reduction of current indicates the increase of resistance after the NH<sub>3</sub> adsorption, which can be directly measured in the experiment. While an opposite trend of current change is displayed in the negative bias region (figure 4(e)). We notice that the decreased current value in the positive bias is much larger than the increased value in the negative bias, which implies that the heterojunction response to NH<sub>3</sub> is rely on the bias direction.

To understand the effect of NH<sub>3</sub> adsorption on the transport properties, we consider the bias dependent transmission spectra of the heterojunction with and without the NH<sub>3</sub> adsorption. Figure 4(f) shows the transmission spectra at 0 V and  $\pm 2.2$  V. We start from the case of zero bias. It is seen that there is a region of zero transmission around the Fermi level with a width of 1.6 eV, which is near the value of the band gap of the heterojunction. Beyond this region, it is clear that the transmission ability decreased below the Fermi level especially in the region of around  $-1.5$  eV and increased slightly above the Fermi level by the NH<sub>3</sub> adsorption. We consider that the reduced and increased transmission abilities have contribution to the reduction and increment of passing current under the positive and negative bias, respectively. When the bias is applied, the current is mainly attributed to the transmission coefficient around the Fermi level within the bias window. For the transmission spectra of the

heterojunction under the bias 2.2 V, the nonzero transmission peak emerges around the Fermi level and naturally leads to much larger current. However, the peak is vanished due to  $\text{NH}_3$  adsorption, which results in no transmission under the bias window and largely lessens the current. Contrary to the transmission spectra under the positive bias, there is no transmission peak near the Fermi level for the heterojunction under the negative bias. Nevertheless, some faint transmission peak exists near the Fermi level as the  $\text{NH}_3$  adsorbed on the heterojunction, which causes the occurrence of the current.

The adsorption of paramagnetic molecules NO and  $\text{NO}_2$  on the heterojunction induce spin polarization as indicated above, which leads to spin-polarized current. We take heterojunction with the  $\text{NO}_2$  adsorption as a representative example to explore the spin-dependent transport and the I–V curve. The spin-polarized I–V curves for the heterojunction with the  $\text{NO}_2$  adsorption are presented in figure 5 (a). It should be noted that the rectifying directions for both spin-up and -down current are not changed by  $\text{NO}_2$  adsorption and the largest rectification ratio at 2.4 V is 123 and 119, respectively. However, it decreases the spin current in two directions: for example, the current of the heterojunction under the positive bias is 1.4  $\mu\text{A}$ , with the adsorption of paramagnetic  $\text{NO}_2$ , the spin-up and –down current is decreased to 0.24 and 0.59  $\mu\text{A}$ , respectively. The current decline is probably because the  $\text{NO}_2$  adsorption introduces backscattering centers that reduce the electron transmission ability. The evolution of the transmission spectra under bias is also plotted in Figure 5 (b). It is clear to see that the transmission peak exists under the positive bias but disappears under the negative bias, which efficiently controls the passing current and leads the rectifying behavior.

From above discussions, we can see that the molecule adsorption has a great impact on the electronic transport properties of the heterojunction. The changes of the resistance and rectifying behavior are expected to make the heterojunction a good candidate for the gas sensing application. Here, we only consider the lateral heterojunction with a zigzag interface but not involved that with armchair interface, which also have been observed in the experiment. Moreover, the asymmetric doped by the transition metal existed in two sides of the heterojunction is also found in the

experiment and its effect on the molecule adsorption and transport properties will be discussed in further work.

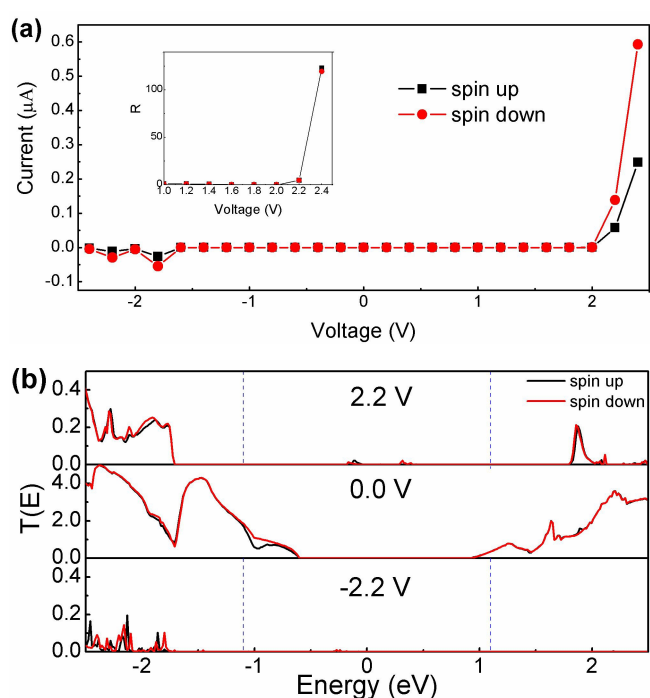


Figure 5. (a) Spin-polarized  $I$ – $V$  curves of heterojunction with the  $\text{NO}_2$  adsorption. The rectification ratio  $R(V)$  is shown in the insets. (b) Transmission spectra in  $0$  V and  $\pm 2.2$  V. The blue dashed lines indicate the bias window for the transportation.

#### 4. CONCLUSIONS

In summary, first principles calculations have been applied to systematically study the geometry, electronic structures, and electron transport properties of the  $\text{MoS}_2/\text{WS}_2$  in-plane heterojunction with and without  $\text{CO}$ ,  $\text{H}_2\text{O}$ ,  $\text{NH}_3$ ,  $\text{NO}$ , and  $\text{NO}_2$  gas molecular adsorption. Our results indicate that the heterojunction is sensitive to gas molecules except  $\text{CO}$  and  $\text{NO}_2$  which possesses the largest binding energy among the gas molecules considered here. This behavior is attributed to the modification of the substrate electronic structure and the charge transfer occurred upon adsorption. Electron transport calculations suggest that the heterojunction possesses an outstanding rectification character. The rectifying direction can be inverted by  $\text{NH}_3$  adsorption and the tunneling resistance can be greatly enhanced. The changes of the resistance and rectifying behavior provide potential applicability for the junction used as gas sensors.

## ACKNOWLEDGEMENTS

We acknowledge the National Nature Science Foundation of China (Grant No. 21573129 and 21403300), the National Nature Science Foundation of Shandong Province (Grant No. ZR2015BQ001), and the General Financial Grant from the China Postdoctoral Science Foundation (Grant No.2013M531595 and 214M560587). The authors also acknowledge a generous grant of computer time from the Norwegian Programme for Supercomputing and the National Supercomputer Center in Tianjin-TianHe-1(A).

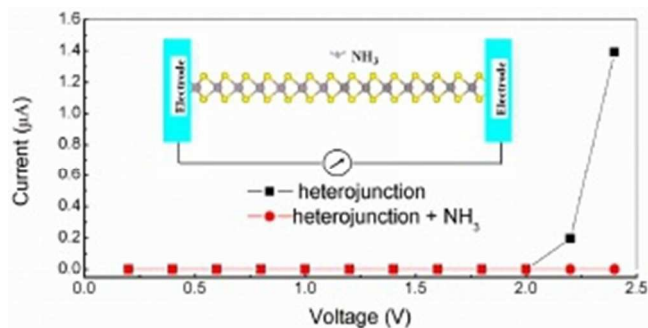
## REFERENCE

- (1). Novoselov, K. S.; Geim, A. K.; Morozov, S. V.; Jiang, D.; Zhang, Y.; Dubonos, S. V.; Grigorieva, I. V.; Firsov, A. A. Electric Field Effect in Atomically Thin Carbon Films. *Science* **2004**, *306*, 666-669.
- (2). Geim, A. K.; Novoselov, K. S. The rise of graphene. *Nature Mater* **2007**, *6*, 183-191.
- (3). Castro Neto, A. H.; Guinea, F.; Peres, N. M. R.; Novoselov, K. S.; Geim, A. K. The electronic properties of graphene. *Rev. Mod. Phys.* **2009**, *81*, 109-162.
- (4). Wang, Q. H.; Kalantar-Zadeh, K.; Kis, A.; Coleman, J. N.; Strano, M. S. Electronics and optoelectronics of two-dimensional transition metal dichalcogenides. *Nature Nanotech.* **2012**, *7*, 699-712.
- (5). Li, L. K.; Yu, Y. J.; Ye, G. J.; Ge, Q. Q.; Ou X. D.; Wu, H.; Feng, D. L.; Chen, X H.; Zhang, Y. B. Black phosphorus field-effect transistors. *Nature Nanotech.* **2014**, *9*, 372-377.
- (6). Coleman, J. N.; Lotya, M.; ÓNeill, A.; D. Bergin, S.; J. King, P. Two-Dimensional Nanosheets Produced by Liquid Exfoliation of Layered Materials. *Science* **2011**, *331*, 568-571.
- (7). Mak, K. F.; Lee, C.; Hone, J.; Shan, J.; F. Heinz, T. Atomically Thin MoS<sub>2</sub>: A New Direct-Gap Semiconductor. *Phys. Rev. Lett.* **2010**, *105*, 136805.

- (8). S. Ross, J.; Klement, P.; M. Jones, A.; J. Ghimire, N.; Yan, J. Q.; Mandrus, D. G.; Taniguchi, T.; Watanabe, K.; Kitamura, K.; Yao, W.; H. Cobden, D.; Xu, X. D. Electrically tunable excitonic light-emitting diodes based on monolayer WSe<sub>2</sub> p-n junctions. *Nature Nanotech.* **2014**, *9*, 268-272.
- (9). M. Jones, A.; Yu, H.; J. Ghimire, N.; Wu, S.; Aivazian, G.; S. Ross, J.; Zhao, B.; Yan, J.; G. Mandrus, D.; Xiao, D.; Yao, W.; Xu, X. D. Optical generation of excitonic valley coherence in monolayer WSe<sub>2</sub>. *Nature Nanotech.* **2013**, *8*, 634-638.
- (10). Yin, Z.; Li, H.; Li, H.; Jiang, L.; Shi, Y.; Sun, Y.; Lu, G.; Zhang, Q.; Chen, X.; Zhang, H. Single-Layer MoS<sub>2</sub> Phototransistors. *ACS Nano* **2012**, *6* (1), 74-80.
- (11). Yoon, Y.; Ganapathi, K.; Salahuddin, S. How Good Can Monolayer MoS<sub>2</sub> Transistors Be? *Nano Lett.* **2011**, *11*, 3768-3773.
- (12). Radisavljevic, B.; B. Whitwick, M.; Kis, A. Small-signal amplifier based on single-layer MoS<sub>2</sub>. *Appl. Phys. Lett.* **2012**, *101*, 043103.
- (13). Radisavljevic, B.; Radenovic, A.; J. Brivio; Giacometti, V.; Kis, A. Single-layer MoS<sub>2</sub> transistors. *Nature Nanotech.* **2011**, *6*, 147-150.
- (14). Kang, J.; Tongay, S.; Zhou, J.; Li, J.; Wu, J. Band offsets and heterostructures of two-dimensional semiconductors. *Appl. Phys. Lett.* **2013**, *102*, 012111.
- (15). Kang, J.; Sahin, H.; M. Peeters, F. Tuning Carrier Confinement in the MoS<sub>2</sub>/WS<sub>2</sub> Lateral Heterostructure. *J. Phys. Chem. C* **2015**, *119*, 9580-9586.
- (16). Gong, Y.; L, J.; Wang, X.; Shi, G.; Lei, S.; Lin, Z.; Zou X.; Ye, G.; Vajtai, R.; I. Yakobson, B.; Terrones, H.; Terrones, M.; Tay, B. K.; Lou, J.; T. Pantelides, S.; Liu, Z.; Zhou, W.; M. Ajayan, P. Vertical and in-plane heterostructures from WS<sub>2</sub>/MoS<sub>2</sub> monolayers. *Nature Mater* **2014**, *13*, 1135-1142.
- (17). Huang, C.; Wu, S.; M. Sanchez, A.; J. P. Peters, J.; Beanland, R.; S. Ross, J.; Rivera, P.; Yao, W.; H. Cobden, D.; Xu, X. D. Lateral heterojunctions within monolayer MoSe<sub>2</sub>-WSe<sub>2</sub> semiconductors. *Nature Mater* **2014**, *13*, 1096-1101.
- (18). Duan, X.; Wang, C.; C. Shaw, J.; Cheng, R.; Chen, Y.; Li, H.; Wu, X.; Tang, Y.; Zhang, Q.; Pan, A.; Jiang, J.; Yu, R.; Huang, Y.; Duan, X. Lateral epitaxial growth of two-dimensional layered semiconductor heterojunctions. *Nature Nanotech.* **2014**, *9*, 1024-1030.

- (19). Gong, Y.; Lei, S.; Ye, G.; Li, B.; He, Y.; Keyshar, K.; Zhang, X.; Wang, Q.; Lou, J.; Liu, Z.; Vajtai, R.; Zhou, W.; M. Ajayan, P. Two-Step Growth of Two-Dimensional WSe<sub>2</sub>/MoSe<sub>2</sub> Heterostructures. *Nano Lett.* **2015**, *15*, 6135-6141.
- (20). SCHEDIN, F.; GEIM, A. K.; MOROZOV, S. V.; HILL, E. W.; BLAKE, P.; KATSNELSON, M. I.; NOVOSELOV, K. S.. Detection of individual gas molecules adsorbed on graphene. *Nature Mater* **2007**, *6*, 652-655.
- (21). Leenaerts, O.; Partoens, B.; Peeters, F. M. Adsorption of H<sub>2</sub>O, NH<sub>3</sub>, CO, NO<sub>2</sub>, and NO on graphene: A first-principles study. *Phys.Rev. B* **2008**, *77*, 125416.
- (22). Xia, W. Q., Hu, W.; Li, Z. Y.; Yang, J. L. A first-principles study of gas adsorption on germanene. *Phys. Chem. Chem. Phys* **2014**, *16*, 22495-22498.
- (23). Kou, L. Z.; Frauenheim, T.; Chen, C. F. Phosphorene as a Superior Gas Sensor: Selective Adsorption and Distinct I-V Response. *J. Phys. Chem. Lett.* **2014**, *5*, 7.
- (24). Li, H.; Yin, Z. Y.; He, Q. Y.; Li, H.; Huang, X.; Lu, G.; Fam, D. W. H.; Tok, A. I. Y.; Zhang, Q.; Zhang, H. Fabrication of Single- and Multilayer MoS<sub>2</sub> Film-Based Field-Effect Transistors for Sensing NO at Room Temperature. *Small* **2012**, *8* (1), 63-67.
- (25). He, Q. Y.; Zeng, Z. Y.; Yin, Z. Y.; Li, H.; Wu, S. X.; Huang, X.; Zhang, H. Fabrication of Flexible MoS<sub>2</sub> Thin-Film Transistor Arrays for Practical Gas-Sensing Applications. *Small* **2012**, *8* (19), 2994-2999.
- (26). Late, D. J.; Huang, Y. K.; Liu, B.; Acharya, J.; Shirodkar S. N.; Luo, J. J.; Yan A. M.; Charles, D.; Waghmare, U. V.; Dravid, V. P.; Rao, C. N. R. Sensing Behavior of Atomically Thin-Layered MoS<sub>2</sub> Transistors. *ACS Nano* **2013**, *7* (6), 4879-7891.
- (27). Huo, N. J.; Yang, S.X.; Wei, Z. M.; Li, S. S.; Xia, J. B.; Li, J. B. Photoresponsive and Gas Sensing Field-Effect Transistors based on Multilayer WS<sub>2</sub> Nanoflakes. *Sci. Rep.* **2014**, *4*, 5209.
- (28). Cho, B.; Hahm, M. G.; Choi, M.; Yoon, J.; Kim, A. R.; Lee, Y. J.; Park, S. J.; Kwon, J. D.; Kim, C. S.; Song, M.; Jeong, Y.; Lee, K. S. N. S.; Yoo, T. J.; Kang, C. G.; Lee, B. H.; Ko, H. C.; Ajayan, P. M.; Kim, D. H. Charge-transfer-based Gas Sensing Using Atomic-layer MoS<sub>2</sub>. *Sci. Rep.* **2015**, *5*, 8052.

- (29). Yue, Q.; Shao, Z. Z.; Chang, S. L.; Li, J. B. Adsorption of gas molecules on monolayer MoS<sub>2</sub> and effect of applied electric field. *Nanoscale Res. Lett.* **2013**, *8*, 425.
- (30). Zhao, S. J.; Xia, J. M.; Kang, W. Gas adsorption on MoS<sub>2</sub> monolayer from first-principles calculations. *Chem. Phys. Lett.* **2014**, *595*, 35-42.
- (31). Kresse, G.; Hafner, J. Ab initio molecular dynamics for liquid metals. *Phys.Rev. B* **1993**, *47*, 558-561.
- (32). Perdew, J. P.; Burke, K.; Ernzerhof, M.. Generalized Gradient Approximation Made Simple. *Phys. Rev. Lett.* **1996**, *77 (18)*, 3865-3868.
- (33). GRIMME, S. Semiempirical GGA-Type Density Functional Constructed with a Long-Range Dispersion Correction. *Comput. Chem.* **2006**, *27*, 1787-1799.
- (34). Brandbyge, M.; Mozos, J. L.; Ordejón, P.; Taylor, J.; Stokbro, K. Density-functional method for nonequilibrium electron transport. *Phys.Rev. B* **2002**, *65 (165401)*, 165401.
- (35). BARONE, V.; CASARIN, M.; FORRER, D.; PAVONE, M.; SAMBI, M.; VITTADINI, A. Role and Effective Treatment of Dispersive Forces in Materials: Polyethylene and Graphite Crystals as Test Cases. *J. Comput. Chem.* **2008**, *30*, 934-939.
- (36). Garcia-Lastra, J. M.; Rubio, C. R. A.; Thygesen, K. S. Polarization-induced renormalization of molecular levels at metallic and semiconducting surfaces. *Phys.Rev. B* **2009**, *80 (245427)*.
- (37). Zhao, J. J.; Buldum, A.; Han, J.; Lu, J. P. Gas molecule adsorption in carbon nanotubes and nanotube bundles. *Nanotechnology* **2002**, *13*, 195-200.



85x42mm (96 x 96 DPI)